J Mater Sci (2008) 43:1958–1965
DOI 10.1007/s10853-008-2460-1

Dual templates assisted preparation and characterization of highly thermostable multicomponent mesoporous material La–Ce–Co–Zr–O used for low-temperature CO oxidation

Zhi-Qiang Zou · Ming Meng · Yu-Qing Zha · Yong Liu

Received: 1 November 2007 / Accepted: 8 January 2008 / Published online: 30 January 2008

Abstract The multicomponent materials La–Ce–Co–Zr–O were first prepared by using mixed surfactants comprised of p-octyl polyethylene glycol phenyl ether (OP) and cetyltrimethyl-ammonium bromide (CTAB) as co-templates, which show large specific surface areas (up to 163 m^2/g) and uniform pore size distributions (3.4–3.6 nm) after calcination at 500 °C. High-resolution transmission electron microscopy (HR-TEM) image shows that these materials possess wormhole-like mesoporous structures. N_2 adsorption/desorption indicates that the coexistence of La and Ce in a proper atomic ratio is very crucial to improve the thermal stability of these mesoporous materials. The catalyst with La/Ce atomic ratio of 1/16 exhibits the best thermal stability. After calcination at 700 °C, its specific surface area is still up to 54 m^2/g, much larger than those for the most reported $LaCoO_3$-related perovskite. Temperature-programed reduction (H_2-TPR) results show that the coexistence of La and Ce in a ratio of 1/16 can bring more profound Co–Ce interaction and the highest mobility of Co–O bond in the catalyst calcined at 700 °C. The mesoporous material La–Ce–Co–Zr–O with La/Ce atomic ratio of 1/16 exhibits not only high-thermal stability, but also novel catalytic activity for CO oxidation.

Introduction

During the cold-start period of vehicles, 50–80% of CO and hydrocarbons were directly released into the air due to the low temperatures of the catalyst-bed and the exhaust itself (<200 °C) at which the three-way catalysts (TWCs) do not work [1]. Therefore, it is necessary to explore novel oxidation catalysts for the removal of the pollutant CO and hydrocarbons at relatively low temperatures. Cobalt oxide is attractive for the preparation of oxidation catalysts because of its high activity for CO oxidation [2, 3]. Besides, it is well known that zirconia is often used as supports for many catalysts because of its good resistance to sintering at high temperatures [4]. At the same time, lanthanum is often added to catalysts as a promoter to improve their component dispersion [5]. Therefore, in our previous study [6], the ternary oxides catalyst La–Co–Zr–O was prepared. However, as it is known that ceria is always used in the TWCs due to its oxygen storage capacity provided by the redox couple Ce^{4+}/Ce^{3+} [7]. So, it is a feasible idea to develop oxidation catalysts based on Co and Zr promoted by La and Ce simultaneously and this interesting combination has not been reported before.

In our previous study [6], a new method involving surfactants participated in the co-precipitation process was used to prepare ternary oxide catalysts La–Co–Zr–O. It has been demonstrated that this novel method is superior to the conventional co-precipitation method, and the catalysts prepared by using mixed surfactants comprised of p-octyl polyethylene glycol phenyl ether (OP) and cetyltrimethyl-ammonium bromide (CTAB) have shown preferable activities compared with those synthesized only using CTAB as sole template. However, the microstructure of this kind of materials still remains unclear. In order to further improve the activity as well as the thermal stability of such materials and understand their microstructures, in the present study, La and Ce simultaneously promoted multicomponent mesoporous catalysts La–Ce–Co–Zr–O were prepared. In order to optimize the catalyst formula,

Z.-Q. Zou · M. Meng (✉) · Y.-Q. Zha · Y. Liu
Department of Catalysis Science and Technology, School of Chemical Engineering and Technology, Tianjin University, Tianjin 300072, P.R. China
e-mail: mengm@tju.edu.cn

different atomic ratios of La/Ce were adjusted during preparation process. The techniques of N_2 adsorption/desorption, high-resolution transmission electron microscopy (HR-TEM) and scanning electron microscopy (SEM) were employed to characterize the materials in order to understand their microstructure. The function of La and Ce, and the correlation between the structures of the catalysts and their oxidation activities were discussed in detail.

Experimental

Catalyst preparation

At first, the La–Ce–Co citrate complex precursor was prepared from appropriate amounts of $La(NO_3)_3{\cdot}6H_2O$, $Ce(NO_3)_3{\cdot}6H_2O$, 1.45 g of $Co(NO_3)_2{\cdot}6H_2O$, 1.92 g of citric acid (atomic ratio (La + Ce)/Co = 1) and 100 mL of distilled water. The surfactants CTAB (4.67 g) and p-octyl polyethylene glycol phenyl ether (4.14 g) were dissolved into 120 g of distilled water and 30 g of HCl 10 wt%. Then the La–Ce–Co citrate complex precursor and 4.28 g of $Zr(NO_3)_4{\cdot}5H_2O$ (atomic ratio Zr/Co = 2) dissolved in 100 mL of distilled water were added, giving a clear homogeneous solution. The mixture was continuously stirred for 2 h, followed by quick addition of 80 mL of 2 M NaOH under vigorous stirring to form a solid precipitate. The pH was adjusted to around 12.5. The resulting gel mixture was stirred for 6 h at room temperature and subsequently transferred to Teflon autoclaves, keeping at 120 °C for 24 h to increase the degree of condensation. The solid product was filtered, washed with water and ethanol, dried in air at 110 °C and finally calcined in air at different temperatures for 4 h. The catalysts are denoted as LCCZ(x)-y, where: LCCZ = La–Ce–Co–Zr oxides, and x is the atomic ratio of La/Ce, while y is the calcination temperature (centigrade). For comparison, the samples free of La or Ce were also prepared, denoted as CCZ-y and LCZ-y, respectively. Here it should be pointed out that the amounts of Co and Zr in all the samples are 0.05 mol and 0.1 mol, respectively. The total amount of La and Ce in the samples is 0.05 mol while the atomic ratio of La/Ce varies from 0 to 1 in different samples.

Nitrogen adsorption/desorption (BET)

The measurement of the specific surface area (S_{BET}) and the pore diameter distribution was carried out at 77 K on a Quantachrome Nova 2000 Series by using the nitrogen adsorption/desorption method. The samples were pretreated in vacuum at 200 °C for 8 h before experiments.

X-ray diffraction (XRD)

X-ray diffraction patterns were recorded on an X'pert Pro diffractometer (PANAlytical Company) with a rotating anode using Co Kα as radiation source (λ=1.7902 Å) at 40 kV and 40 mA. The data of 2θ from 10° to 90° range were collected with the step size of 0.02°.

HR-TEM and SEM

The pore structure of the catalyst was measured using a high-resolution transmission electron microscope (HR-TEM, Philips Tecnai G^2F20), which was operated at 200 kV. SEM analyses were carried out with a XL30ESEM microscope, operating with an accelerating voltage of 20 kV.

Temperature-programed reduction (TPR)

Temperature-programed reduction measurement was conducted on a TPDRO 1100 apparatus supplied by Thermo-Finnigan company. Each time, 30 mg of the sample was heated from room temperature to 900 °C at a rate of 10 °C/min. A mixture gas of H_2 and N_2 (H_2/N_2 molar ratio: 5%) was used as reductant with a flow rate of 20 mL/min.

Evaluation of catalytic performance

The catalytic activities of the samples for CO oxidation were measured in a fixed-bed quartz tubular reactor (i.d. 8 mm) mounted in a tube furnace equipped with K-type thermocouples. The temperature slope for the catalyst bed is 5 °C/min. Each time, about 900 mg of catalyst (40–60 mesh) was placed into the reactor tube. The reaction mixtures containing 1.0 vol% CO, 5 vol% O_2, and balance of N_2 are fed to catalyst bed at a space velocity of 20,000 h^{-1}. The effluent gas from the reactor was analyzed by a gas chromatograph (BFS, SP 3430) equipped with a thermal conductivity detector and a flame ionization detector. The CO conversions were measured after keeping the catalysts at given temperatures for 10 min.

Results and discussion

Specific surface areas and pore distributions

Figure 1 shows the nitrogen adsorption/desorption isotherms of all the samples. The isotherms for the samples calcined at 500 °C exhibit a typical IV shape as defined by IUPAC [8], with an evident H-2 type hysteresis loop, implying the presence of mesoporous structure in the

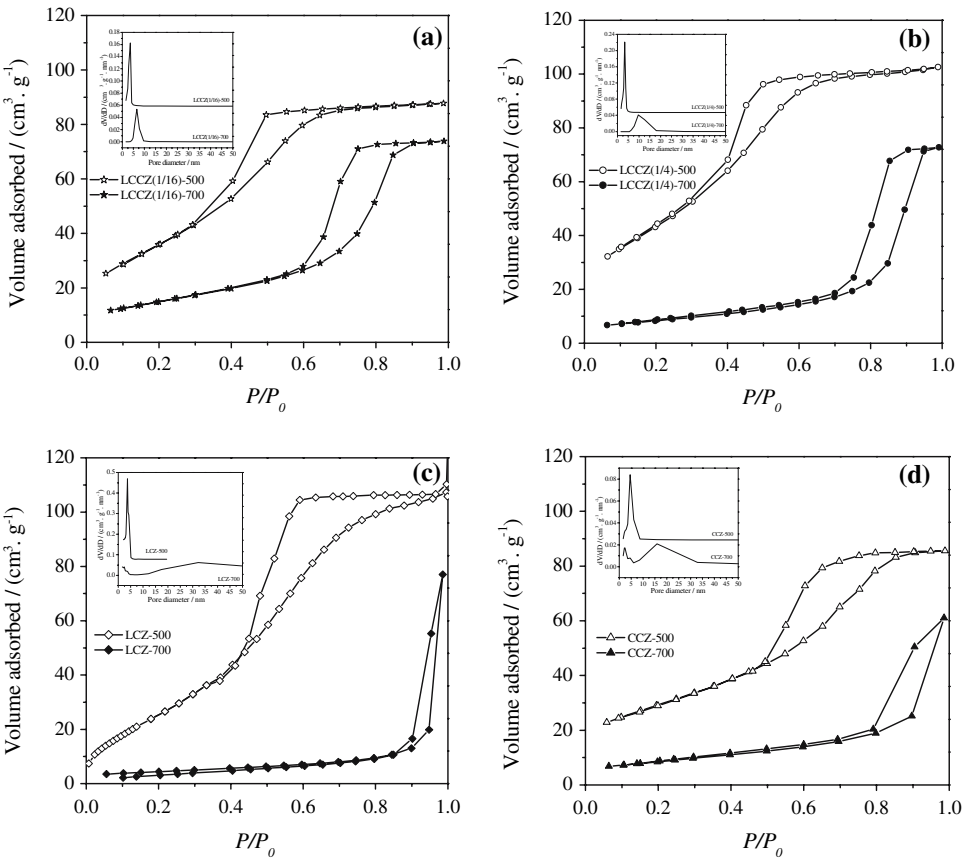

Fig. 1 Nitrogen adsorption/desorption isotherms and pore diameter distributions (inset) of the samples

samples. From the inset figures of Fig. 1, it can be seen that the BJH pore size distributions of all the samples calcined at 500 °C are narrow, implying the textural uniformity of the samples. It is worth noting that when the calcination temperature is increased to 700 °C, the H-2 type hysteresis loops are also observed for the samples LCCZ(1/16)-700 and LCCZ(1/4)-700, but the hysteresis loops for the samples LCZ-700 and CCZ-700 are more similar to H-3 type hysteresis loop, which indicates that the two samples contain more interparticular pores and have lost most of the inner mesoporosity. These two H-3 type hysteresis loops occur at very high relative pressures (>0.8), implying a very wide pore size distribution, as shown in Fig. 1(c) and (d) (see inset). Moreover, it can also be found that the pore size distribution for the sample LCZ-700 is extremely wide with some pores exceeding mesopore range.

The texture data of the samples are summarized in Table 1. It is found that all the samples calcined at 500 °C exhibit high specific surface areas above 100 m^2/g. The samples containing La and Ce simultaneously, calcined at 500 °C, show much larger specific surface areas than those free of La or Ce. With the increase of calcination temperature, the specific surface areas decrease. However, the sample with La/Ce atomic ratio of 1/16 shows the best thermal stability, which can retain a satisfactory specific surface area of 54 m^2/g after calcination at 700 °C, while others show much lower values less than 30 m^2/g. It is well known that the most reported Co-based oxidation catalyst is $LaCoO_3$ perovskites with or without other metals doped. However, these catalysts often show very low surface areas. For instance, Tanaka et al. [9] reported that their $La_{0.9}Ce_{0.1}CoO_3$ catalyst also calcined at 700 °C possessed the surface area of only 20.6 m^2/g. In the present work, the coexistence of La and Ce gives bigger specific surface areas for the samples calcined at 500 °C, and a proper La/Ce atomic ratio (1/16) ensures a satisfactory specific surface area and relatively narrow pore size distributions when the sample is treated at higher temperature of 700 °C. The La and Ce atoms may have effectively prevented particles agglomeration during thermal treatment, and partly maintain inner mesoporous structure even after calcination at 700 °C. However, when the content of La is increased, the specific surface area of the sample calcined at 700 °C decreases more obviously probably due to the agglomeration of the high-content La oxide itself. Therefore, the coexistence of La and Ce in a proper ratio is a key factor for keeping high specific surface area and narrow pore size distribution of the samples calcined at 500 °C or 700 °C.

Table 1 Physical structure data of the samples

Sample	S_{BET} (m^2/g)	Pore diameter (nm)	Pore volume (cm^3/g)	Crystallite sizes (nm)	
				Co_3O_4	ZrO_2
LCZ-500	118	3.7	0.17	18.7	Amorphous
CCZ-500	105	4.6	0.13	19.4	4.0
LCCZ(1/4)-500	163	3.4	0.17	17.4	3.0
LCCZ(1/16)-500	138	3.6	0.15	15.5	3.6
LCZ-700	16	32.3	0.12	29.4	9.4
CCZ-700	30	15.9	0.10	23.9	8.0
LCCZ(1/4)-700	30	9.6	0.12	24.3	5.7
LCCZ(1/16)-700	54	6.6	0.12	23.7	6.1

XRD

The XRD patterns of the samples LCCZ(x)-y, LCZ-y, and CCZ-y are shown in Fig. 2. Well-defined features of Co_3O_4 crystalline phase are evident in all samples and the peaks at $2\theta = 43.1°$ corresponding to the first strongest diffraction peak of Co_3O_4 (PCPDFWIN, No.78–1970) are intensified with the increase of calcination temperature from 500 °C to 700 °C, indicating the growing of Co_3O_4 crystallites, which has been quantitatively calculated by the Sherrer's equation on the basis of reflection [311] ($2\theta = 43.1°$), as listed in Table 1. Tetragonal ZrO_2 is also observed in all the samples except LCZ-500, the peak of which is quite broad, implying the presence of some amorphous phase in it. The size of ZrO_2 crystallites in Table 1 was obtained on the basis of reflection [112] ($2\theta = 58.0°$). Similar to Co_3O_4, the crystal ZrO_2 also grows with the increase of calcination temperature from 500 °C to 700 °C.

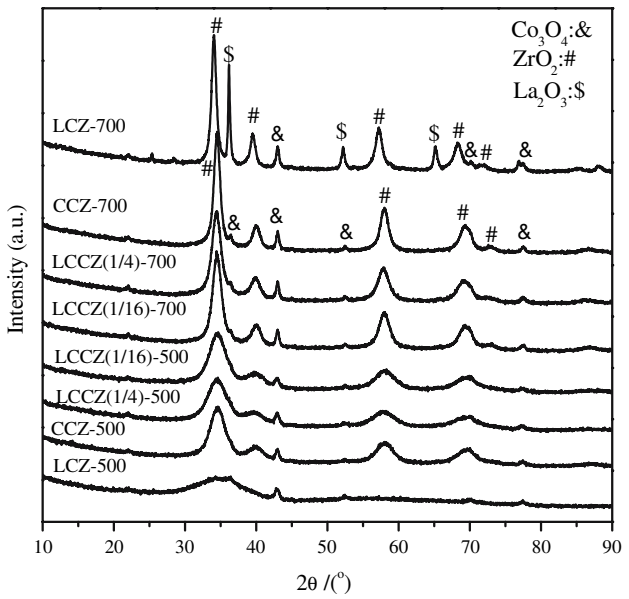

Fig. 2 XRD patterns of the samples

It is found that La_2O_3 ($2\theta = 36.0°$, 52.2°, 65.2°) is only noticed in the sample LCZ-700 due to its much larger amount of La in this sample than in other samples calcined at 700 °C. However, these three peaks may also include the diffraction effect of Co_3O_4 since that the standard diffraction pattern of Co_3O_4 also has peaks at $2\theta = 36.5$, 52.5, and 65.6° which are very close to those of La_2O_3. Although there is also a very small but visible shoulder peak at $2\theta = 36.4°$ for the sample CCZ-700, which is very close to the strongest peak of La_2O_3 at $2\theta = 36.0°$, this peak cannot be ascribed to La_2O_3 since this sample does not contain La at all. So, this peak only should be assigned to Co_3O_4 phase. Inspection of Fig. 2 and the results above reveals that the higher the calcination temperature, the sharper the diffraction peaks, indicating the sintering of the samples. It is worth noting that this tendency is more obvious for the sample free of Ce by comparison of the peaks of each sample calcined at 500 °C and 700 °C, which implies that the addition of CeO_2 can markedly inhibit the sintering of the components. Only from the XRD results, it seems that the content of La has neglectable effects on the Ce-containing samples.

HR-TEM and SEM

The TEM image of the sample LCCZ(1/16)-500 is shown in Fig. 3. It can be seen that this image exhibits a uniform mesopore size with a wormhole-like structure lacking a long range packing order as reported for MSU or DWM compounds [10, 11]. At the same time, no small angle X-ray diffraction signal is observed for this material, which means that the uniformity in pore size does not imply bi- or three-dimensional X-ray detectable ordering [12]. Other samples have the similar structures, whose images are not shown.

It is well known that the ordered mesoporous materials, such as MCM-41, MCM-48, etc., possess not only uniform pore diameter but also well-defined channels [13, 14]. In this work, the catalyst La–Ce–Co–Zr–O is actually a

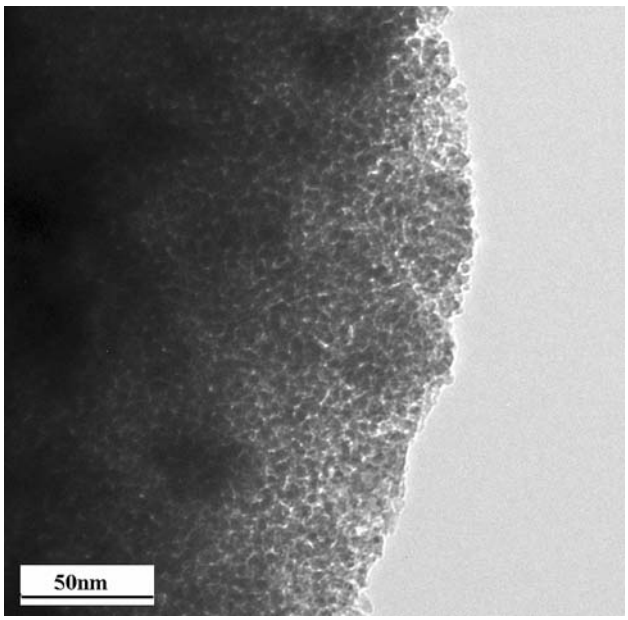

Fig. 3 HR-TEM image of the sample LCCZ(1/16)-500

mixture of disordered mesoporous oxides as observed from XRD, which only possesses uniform mesoporous diameter, but no well-defined channel structure. Generally, the pore diameter is closely related to the used surfactants and calcination temperatures, while the well-defined channel structure strongly depends on the regular framework formed by Si–O–Si or Si–O–Al tetrahedron, such as in MCM-41 (meso-material) or Y zeolite (micro-material). In the catalyst La–Ce–Co–Zr–O, La, Ce, Co, and Zr show different properties from Si and Al, so, no formation of well-defined channel is intelligible. The uniform pore diameter should be ascribed to the participation of the surfactants OP and CTAB. The removal of the surfactants during calcination leaves pores in the samples and the simultaneous introduction of OP and CTAB should increase the pore diameter which has been discussed in particular in our previous study [6]. Actually, in view of catalysis, the regular channel structure is sometimes not very necessary, while the proper pore size seems more important for mass transfer. Here, the La–Ce–Co–Zr–O catalysts are typical wormhole-like mesoporous materials, but this kind of interconnected mesoporous channels should favor the transport of reactants and products.

The SEM images of the samples calcined at 700 °C displayed in Fig. 4 indicate that the morphology of the catalysts is closely related to their composition. The sample LCZ-700 shows very compact aggregates with some sheets on it, while the sample CCZ-700 exhibits very inhomogeneous and irregular particles with evident edges and corners. When La and Ce are contained in the sample simultaneously, more homogeneous particle aggregates are observed. Especially for the sample LCCZ(1/16)-700, much smaller and well-contacted particles have formed a spongy structure with more exposed sites available, which is favorable to molecule adsorption and mass transport during catalytic process.

H_2-TPR

The oxidative performance of Co_3O_4 has been proposed to follow a redox cycle involving reduction/oxidation of the

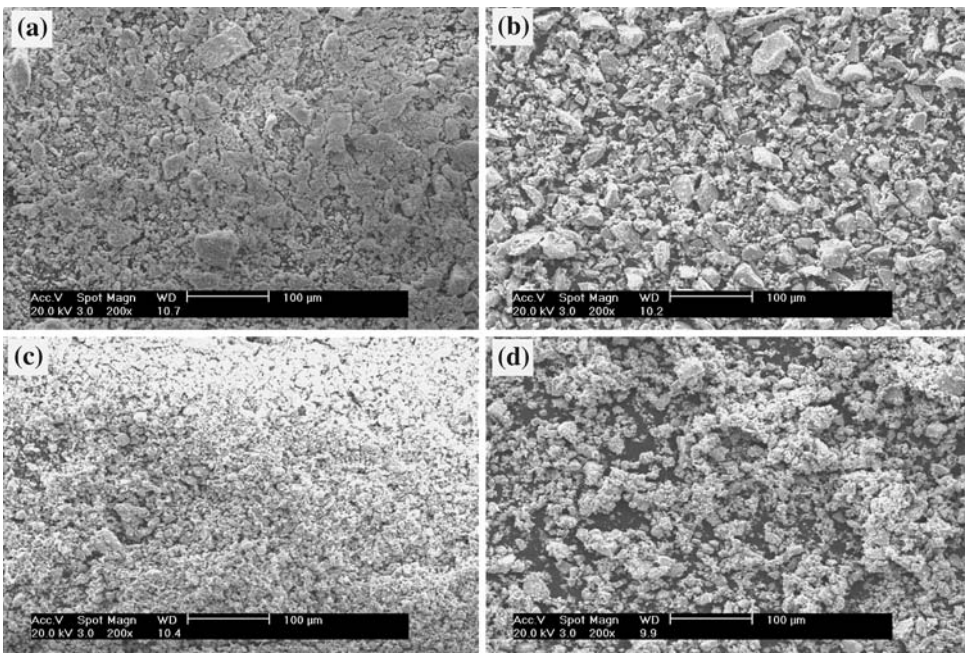

Fig. 4 SEM image of the samples calcined at 700 °C (**a**) LCZ-700; (**b**) CCZ-700; (**c**) LCCZ(1/16)-700; (**d**) LCCZ(1/4)-700

Co^{3+} sites [15]. So, the mobility of Co–O bond is tightly related to its oxidation activity. In order to determine the mobility of Co–O bond in different samples, the H_2-TPR tests were carried out, the results of which are shown in Fig. 5. It can be seen that there are three discernible peaks (labeled as α, β, and γ) for all the samples except sample LCZ-700.

Normally, La_2O_3 and ZrO_2 cannot be reduced by H_2. Therefore, in Fig. 5, all the peaks could be mainly assigned to the reduction of Co_3O_4 while the reduction of CeO_2 may be covered up due to its much lower reducibility than Co_3O_4. Generally, transition metal oxides, like CuO get reduced in a wider temperature range by a two-step stage when contacting with ceria [16, 17]. The first reduction step is always promoted by the interaction between them while the second step is delayed by the stabilization effect of ceria on the cations at the medium valence. Sanchez et al. [18] indicated that there are some oxygen vacancies on the surface of ZrO_2 with fluorite structure, which can be occupied by the supported metal ions. Therefore, after calcination at high temperature, Co ions may have occupied the oxygen vacancies or embed into the fluorite structure of ZrO_2, which makes the reduction of the interacting Co–Zr phases ($Co^{2+} \rightarrow Co^0$) more difficult than normal Co oxide phases. On the basis, the assignment is therefore made as follow:

Peak α: reduction of the highly dispersed Co_3O_4 and/or small crystallite of Co_3O_4 interacting with CeO_2 to CoO;
Peak β: reduction of the XRD-visible, well defined crystalline Co_3O_4 particles to metal Co;
Peak γ: reduction of the Co^{2+} interacting with ZrO_2 and/or CeO_2 to Co^0.

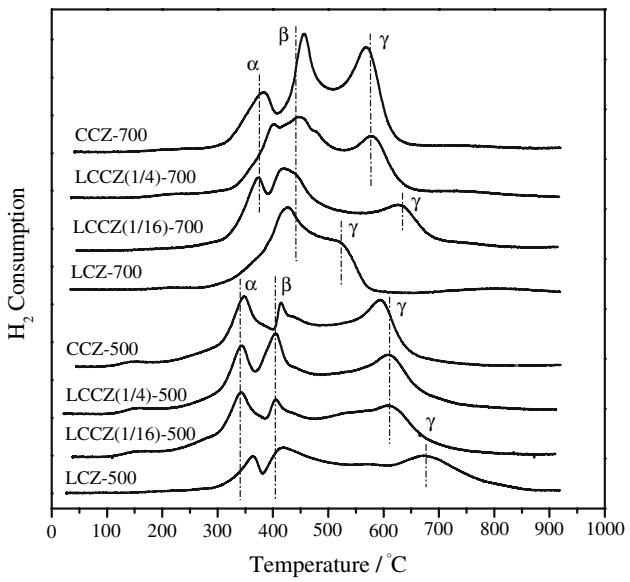

Fig. 5 H_2-TPR profiles of the samples

By comparison of the peaks of all the samples calcined at 500 °C, it can be seen that the temperatures of peak α is highest for the samples LCZ-500 free of Ce, due to lack of the promotion effect of Ce to the reduction of Co oxides, which implies the least mobility of Co–O bond and poor catalytic activity of this catalyst. With the increase of calcination temperatures, peak α and β of all samples have shifted to higher temperatures. For sample LCZ-700, the peak α has almost disappeared, suggesting that the surface highly dispersed Co_3O_4 crystallites have converted to larger bulk Co_3O_4. It is noticeable that there are no significant differences for peak α among the Ce-containing samples calcined at 500 °C while the differences are greatly magnified when the calcination temperature is increased to 700 °C. The temperature of peak α for the sample LCCZ(1/16)-700 is the lowest, suggesting that the La addition in a proper ratio can further promote the reduction of Co_3O_4 in the Ce-containing sample.

By inspection of peak γ of all the samples calcined at 700 °C, it is found that the temperatures of this peak for the samples containing La and Ce simultaneously are higher than those of the samples free of La or Ce, especially for the sample LCCZ(1/16)-700. But the temperature of peak α in this sample is the lowest. The reason may be surmised that an easier contact between Co and Ce phase occurs on this sample, and the stronger Co–Ce interacting could promote the reduction of Co^{3+} to Co^{2+}, but delay the reduction of Co^{2+} to Co^0. However, the reduction/oxidation of the Co^{3+} sites to Co^{2+} mainly accounts for the oxidation performance of Co_3O_4. So, the reduction characteristic of peak α determines the catalytic activity of the samples to a greater extent than that of peak γ.

In summary, from Fig. 5 and the analysis above, it can be concluded that the samples free of Ce exhibit the worst ability to reduce Co^{3+} to Co^{2+}, suggesting that the reduction of cobalt oxide is favored when ceria is present. After thermal treatment at 700 °C, the sample LCCZ(1/16)-700 shows the best reducible ability, probably due to more profound Co–Ce interaction resulting from the coexistence of La and Ce with a proper ratio. Based upon the H_2-TPR results, it is deduced that the sample with La/Ce atomic ratio of 1/16 should have the best oxidative performance compared with other samples calcined at 700 °C, which is verified in the next section.

Catalytic performance for CO oxidation

The catalytic activities for CO oxidation of the fresh samples are shown in Fig. 6. Here it should be pointed out that in this work, the samples with La/Ce ratios of 1/32 and 1/8 have also been prepared and it is found that their activities for CO oxidation are inferior to that of sample

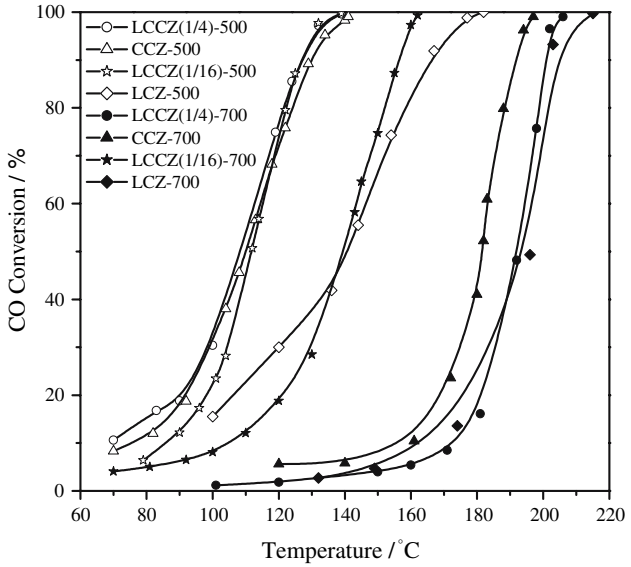

Fig. 6 The CO oxidation activities of the samples

LCCZ(1/16) (not shown). From Fig. 6, it can be seen that among all the samples calcined at 500 °C, only the one free of Ce shows lower activity than other samples. The least mobility of Co–O bond inferred from the H_2-TPR results mainly accounts for the low activity of the sample LCZ-500. In addition, lack of CeO_2 also decreases the ability of the catalyst for activating and transferring oxygen species during reaction. All the Ce-containing samples calcined at 500 °C show similar high activities for CO oxidation.

When the calcination temperature is increased from 500 °C to 700 °C, the activities of all the samples decrease, induced by the declined specific surface areas, the growing crystal size of Co_3O_4 and higher reduction temperatures of Co_3O_4, illustrated in the section of N_2 adsorption/desorption, XRD and H_2-TPR. However, the sample LCCZ(1/16)-700 still shows considerable activity. The temperature for 100% conversion of CO is about 162 °C, while the corresponding temperatures over other samples have exceeded 195 °C. The La and Ce simultaneously promoted catalyst with a ratio of 1/16 shows not only much better thermal stability, but also high oxidation activity than the catalysts free of La or Ce. Taking into account the characterization results, the main reasons leading to above significant difference in activity can be described as follows. First, the sample with La/Ce atomic ratio of 1/16 possesses the largest specific surface area (54 m^2/g) and still keeps its homogeneous mesoporous structure when calcined at 700 °C. The results of SEM also indicate that this sample is comprised of smaller and well-contacted particles with more active sites exposed. Second, the H_2-TPR results show that in the low temperature region (<500 °C), the active phase Co_3O_4 in this sample is reduced at lower temperatures due to more profound Co–Ce interaction than in other samples, which suggests that the activation of Co–O bond in this sample is easier, as is helpful to increase the oxidation activities of the catalyst.

Conclusions

The multicomponent oxides catalysts La–Ce–Co–Zr–O were first prepared by using mixed surfactants comprised of p-octyl polyethylene glycol phenyl ether (OP) and CTAB as co-templates. These multicomponent catalysts exhibit wormhole-like mesoporous structures with uniform pore size (3.4–3.6 nm), and their specific surface areas are very high (up to 163 m^2/g). The coexistence of La and Ce exerts great physical and chemical effect on this kind of materials. In physical aspect, only the coexistence of La and Ce can keep the inner mesoporous structures and high specific surface areas after thermal treatment at relatively high temperature. In addition, the atomic ratio of La/Ce is very crucial. The sample with La/Ce atomic ratio of 1/16 shows the best thermal stability, whose surface area (54 m^2/g) and mesoporous structures are well maintained even after calcination at 700 °C. In chemical aspect, H_2-TPR results indicate that Ce addition can obviously promote the reduction of active phase Co_3O_4 due to Co–Ce interaction while La addition in a proper atomic ratio of La/Ce can further improve the reducibility of Co_3O_4. As a result, the La and Ce simultaneously promoted catalyst with La/Ce ratio of 1/16 exhibits the highest thermal stability and the best activity for low-temperature CO oxidation.

Acknowledgements This work is financially supported by the National Natural Science Foundation of China (No. 20676097), the "863 Program" of the Ministry of Science & Technology of China (No.2006AA06Z348), and the Program for New Century Excellent Talents in University of China (NCET-07-0599). The authors are also grateful to the support from the Natural Science Foundation of Tianjin (No.05YFJMJC09700), the Specialized Research Fund for the Doctoral Program of Higher Education of China (No. 20040056028) and the Cheung Kong Scholar Program for Innovative Teams of the Ministry of Education (No. IRT0641).

References

1. Summers JC, Sawyer JE, Frost AC (1992) ACS Symp Paper 495:98
2. Thormählen P, Skoglundh M, Fridell E, Andersson B (1999) J Catal 188:300
3. Jansson J (2000) J Catal 194:55
4. Wyrwalski F, Lamonier JF, Siffert S, Gengembre L, Aboukaïs A (2007) Catal Today 119:332
5. Gunasekaran N, Saddawi S, Carberry JJ (1996) J Catal 159:107
6. Zou ZQ, Meng M, Luo JY, Zha YQ, Xie YN, Hu TD, Liu T (2006) J Mol Catal A 249:240
7. Graham GW, Jen HW, McCabe RW, Straccia AM, Haack LP (2000) Catal Lett 67:99

8. Sing KSW, Everett DH, Haul RA, Moscow L, Pierotti RA, Rouquerol J, Siemieniewska T (1985) Pure Appl Chem 57:603
9. Tanaka H, Mizuno N, Misono M (2003) Appl Catal A 244:371
10. Prouzet E, Pinnavaia TJ (1997) Angew Chem Int Ed Engl 36:516
11. Blin JL, Léonard A, Su BL (2001) Chem Mater 13:3542
12. Larsen G, Lotero E, Nabity M, Petkovic LM, Shobe DS (1996) J Catal 164:246
13. Beck JS, Vartuli JC, Roth WJ, Leonowicz ME, Kresge CT, Schmitt KD, Chu CTW, Olson DH, Sheppard EW, McCullen SB, Higgins JB, Schlenker JL (1992) J Am Chem Soc 114:10834
14. Shao YF, Wang LZ, Zhang JL, Anpo M (2005) Micropor Mesopor Mater 86:314
15. Jansson J, Palmqvist A, Fridell E, Skoglundh M, Österlund L, Thormählen P, Langer V (2002) J Catal 211:387
16. Martinez-Aris A, Fernandez-Garcia M, Galvez O, Coronado JM, Anderson JA, Conesa JC, Munuera G (2000) J Catal 195:207
17. Fernadez-Garcia M, Rebollo EG, Ruiz AG, Conesa JC, Soria J (1997) J Catal 172:146
18. Sanchez MG, Gazquez JL (1987) J Catal 104:120